

## Article

# Au–Ru Composite for Enzyme-Free Epinephrine Sensing

Maxim S. Panov <sup>1,2</sup> , Alexey P. Zakharov <sup>1</sup>, Evgenia M. Khairullina <sup>1</sup>, Ilya I. Tumkin <sup>1</sup> ,  
Andrey S. Mereshchenko <sup>1</sup> , Dmitrii M. Nikolaev <sup>3,4</sup> , Andrey V. Vasin <sup>3</sup>  and Mikhail N. Ryazantsev <sup>1,3,\*</sup> 

- <sup>1</sup> Institute of Chemistry, Saint Petersburg State University, 26 Universitetskii pr, 198504 Saint Petersburg, Russia  
<sup>2</sup> Center for Biophysical Studies, St. Petersburg State Chemical Pharmaceutical University, Professor Popov Str., 14, Lit. A, 197022 Saint Petersburg, Russia  
<sup>3</sup> Institute of Biomedical Systems and Biotechnologies, Peter the Great St. Petersburg Polytechnic University, 29 Polytechnicheskaya Str., 195251 Saint Petersburg, Russia  
<sup>4</sup> Nanotechnology Research and Education Centre RAS, Saint Petersburg Academic University, 8/3 Khlopina Street, 194021 Saint Petersburg, Russia  
\* Correspondence: mikhail.n.ryazantsev@gmail.com

**Abstract:** We report the synthesis and investigation of Au–Ru composite with highly developed specific surface area exhibiting excellent electrocatalytic performance suitable for detection of such hydrophobic metabolites as epinephrine in the physiological environment. This electrode material was fabricated using two-stage laser-assisted metal deposition technique. The morphological and structural studies of Au–Ru were performed using methods of scanning electron microscopy (SEM), energy-dispersive X-ray spectroscopy (EDX) and X-ray diffraction spectroscopy (XRD). The voltammetric methods, including cyclic voltammetry (CV), differential pulse voltammetry (DPV) and direct amperometry, were used to analyze the composite's electrochemical properties. The Au–Ru sensor exhibited two linear ranges of the non-enzymatic epinephrine detection: 0.01–10  $\mu\text{M}$  and 10–1000  $\mu\text{M}$ . The calculated sensitivities within these two ranges were 32.8 and 3.3  $\mu\text{A } \mu\text{M}^{-1} \text{ cm}^{-2}$ , whereas the corresponding limits of detection were 9 and 20 nM, respectively. The Au–Ru sensor also revealed good stability and reproducibility, as well as high selectivity towards epinephrine detection in the presence of a number of the interfering species.

**Keywords:** laser-induced metal deposition; gold; ruthenium; epinephrine; enzyme-free sensors



**Citation:** Panov, M.S.; Zakharov, A.P.; Khairullina, E.M.; Tumkin, I.I.; Mereshchenko, A.S.; Nikolaev, D.M.; Vasin, A.V.; Ryazantsev, M.N. Au–Ru Composite for Enzyme-Free Epinephrine Sensing. *Chemosensors* **2022**, *10*, 513. <https://doi.org/10.3390/chemosensors10120513>

Academic Editor: Dario Compagnone

Received: 21 October 2022  
Accepted: 29 November 2022  
Published: 3 December 2022

**Publisher's Note:** MDPI stays neutral with regard to jurisdictional claims in published maps and institutional affiliations.



**Copyright:** © 2022 by the authors. Licensee MDPI, Basel, Switzerland. This article is an open access article distributed under the terms and conditions of the Creative Commons Attribution (CC BY) license (<https://creativecommons.org/licenses/by/4.0/>).

## 1. Introduction

New materials sensitive to various important biological analytes are in great demand for different fields of science and industry, including medicine, clinical research and diagnostics of a whole range of serious diseases [1–3]. The detection of hydrophobic biomarkers is of particular interest because of their poor solubility in water [3]. It is known that the concentration of these hydrophobic molecules in biological fluids is very low and, therefore, their precise and selective analysis is extremely difficult. One of the striking examples of such biomarkers is the cationic catecholamine epinephrine (EP or adrenaline,  $\text{C}_9\text{H}_{13}\text{NO}_3$ ) [4]. EP is a very important hormone and neurotransmitter that takes part in many biological processes such as glycogen metabolism [5], regulation of blood pressure [6], etc. Pathological levels of EP (from several to several tens of nM) can indicate the development of very serious diseases (e.g., adrenal cancer [7]). One of the main reasons for the difficulty of epinephrine sensing can be related with simplicity of its oxidation to adrenalinchrome. The latter easily forms polymers that can block the electrode surface [8]. Additionally, catecholamines are known to have a short half-life in blood, therefore, their detectable amounts are quite small [3].

Typical methods used for analysis of EP and other hydrophobic metabolites such as surface enhanced Raman scattering (SERS) spectroscopy [9] and high-performance liquid chromatography (HPLC) [10] exhibit a number of serious drawbacks. Among them are complex procedures for sample preparation and pretreatment, as well as the need to use

expensive equipment that requires a long analysis time. In contrast, the electrochemical methods are decent alternative to the aforementioned approaches [2,3,11]. Indeed, they are quite suitable for biosensing due to their simplicity, low cost, fast response time and high sensitivity. In general, the electrochemical detection of biomolecules can be achieved using two principal approaches [12]. The first approach deals with enzymes used as specific biorecognition elements of biosensors. However, despite the good sensitivity and selectivity demonstrated by enzymatic sensors, they suffer from low stability and reproducibility [12,13]. Moreover, enzymes are expensive and very sensitive to temperature and pH, whereas the procedures of their immobilization are rather complicated and time consuming [14]. On the other hand, the second approach is based on the enzyme-free sensing and can omit the shortcomings mentioned above. In this case, the electrocatalytic oxidation of an analyte occurs directly on the surface of the electrode material [12,15].

Recent progress of materials for enzyme-free sensing of epinephrine was mostly accomplished in the sensitivity enhancement [3]. One of the most remarkable results in this regard were revealed by metallic structures, including precious metals [16], transition metals [17], metal oxides [18], organometallic frameworks [6], etc. Metal composite nanostructures also deserve to be mentioned here due to the high electrocatalytic activity of these materials caused by the presence of a great number of active centers on their surface and the synergetic effect from two different metal elements [19–22]. Nevertheless, ensuring the detection of hydrophobic analytes, including EP, with high reliability and selectivity remains a big challenge. The latter is especially relevant for simultaneous detection of epinephrine and another important neurotransmitter such as dopamine, whose oxidation potential is very similar to that of EP ( $\sim 0.2$  V) [3].

Among the methods suitable for fabrication of the aforementioned electrode materials, laser-assisted methods [23–26] attract a special attention. Their strongest suits are high expressiveness, ability to metallize different substrates and to form metal structures of various geometries, as well as consumption of a small quantity of reagents needed for synthesis [27]. There is another technique related to the laser-based technologies—Laser-induced Chemical Liquid-phase Deposition (LCLD). In this simple and cheap approach, the focused laser light stimulates the metal reduction reaction in the local volume of a solution resulting in formation of porous metallic structures on the surface of different dielectrics. In our previous LCLD experiments, we managed to produce a wide range of the electrode materials based on such metals as copper [28], iridium [29], molybdenum [30] and others [31–33].

The main goal pursued in this work was to develop a laser-assisted synthesis of bimetallic microstructures composed of gold and ruthenium with good electrocatalytic performance towards epinephrine sensing. These two metals are quite promising for biosensing applications because of their good electrical properties, high catalytic activity and great biocompatibility. In addition, their combination with each other can provide excellent results for highly effective enzyme-free sensing due to mutual synergistic interactions. As a result, we were able to fabricate a gold–ruthenium composite that can be used for non-enzymatic detection of small concentrations of EP in the physiological solution with good sensitivity and selectivity.

## 2. Materials and Methods

### 2.1. Laser-Assisted Synthesis of Au–Ru Composite

All chemical reagents (analytically graded) were obtained from Sigma Aldrich (St. Louis, MI, USA). The composition of solutions used for fabrication of the electrode materials based on gold and ruthenium are presented in Table 1.

These materials were fabricated using the simple and cheap LCLD technique. The layout of the experimental setup is shown in Figure 1. Here, the 532 nm output from a diode-pumped continuous-wave solid-state Nd:YAG laser (Changchun, China) was sent to an optical separation cube through two Al mirrors. Then, the laser output was focused with a spot size of 10  $\mu$ m on the front side of the second glass window of the experimental

cell using a standard microscope objective (15 mm focus length). The experimental cell can be moved by a computer-controlled XYZ motorized stage for deposition of metallic structures with different geometry. Further, part of the 532 nm laser beam after reflection from the front side of the cell's first glass window traveled to a web-camera through an optical separation cube, Al mirror and focusing lens. A web-camera was used to control and regulate the metal deposition process. A neutral density filter (fractional transmittance 25%) was used to avoid saturation of a web-camera.

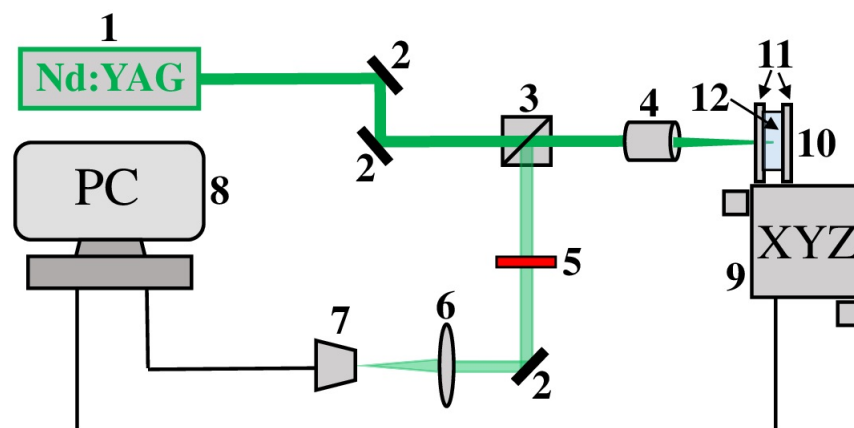


**Figure 1.** The LCLD experimental setup. 1—Nd:YAG 532-nm cw (continuous-wave) laser, 2—Al mirror, 3—optical separation cube, 4—microscope objective, 5—attenuation filter, 6—focusing lens, 7—web-camera, 8—personal computer, 9—XYZ motorized stage, 10—experimental chemical cell, 11—glass window (substrate), 12—chemical solution (see Table 1).

In the current study, the LCLD synthesis of Au-Ru composite was conducted in two stages upon 532-nm irradiation. At the first stage, we deposited gold structures (the Au electrode of the 10-mm length and the  $\sim 100\text{-}\mu\text{m}$  width) on the surface of glass. At the second stage, the fabricated gold electrode was modified by deposition of ruthenium on its surface. The scanning speed in both stages was  $5\ \mu\text{m s}^{-1}$ . The laser power densities used for the composite synthesis were  $\sim 15$  and  $\sim 18\ \text{mW}\ \mu\text{m}^{-2}$  for the first and second steps, respectively. A higher laser power density required for the second stage can be explained by a higher initiation threshold of the ruthenium reduction reaction.

**Table 1.** The composition of solutions used for laser-assisted deposition of Au and Ru structures. In both cases, DMF (*N,N*-dimethylformamide) was used as a solvent.

Electrode Material	Reagent, (mM)	Concentration, (mM)
Au	chloro(triphenylphosphine)gold(I) [(C <sub>6</sub> H <sub>5</sub> ) <sub>3</sub> P]AuCl	3
Ru	triruthenium dodecacarbonyl Ru <sub>3</sub> (CO) <sub>12</sub>	5

## 2.2. Morphology and Composition Analysis

The electron micrographs of Au-Ru composite were obtained using scanning electron microscope Zeiss Supra 40 VP (Oberkochen, Germany). The elemental analysis of this composite was performed using the energy-dispersive X-ray (EDX) analyzer (INCA X-Act, Oxford Instruments, UK).

The X-ray diffraction (XRD) analysis of the Au-Ru composite was accomplished using Bruker D2 Phaser diffractometer operated with LynxEye detector (Karlsruhe, Germany).

The X-ray photoelectron spectroscopy (XPS) measurements were conducted using a spectrometer Escalab 250Xi (Thermo Fisher Scientific, East Grinstead, UK).

### 2.3. Electrochemical Studies

The voltammetric methods were implemented to examine the electrochemical properties of Au–Ru composite. These methods included direct amperometry, cyclic voltammetry (CV) and differential pulse voltammetry (DPV). The synthesized composite was used as a working electrode in a standard three-electrode electrochemical cell. In this cell, the Ag/AgCl electrode and Pt wire were used as reference and counter electrodes, respectively. All measurements were carried out in phosphate-buffered saline background solution (0.1 M PBS, pH 7.0) at room temperature using Corrtest CS300 potentiostat (Woham Corrtest Instruments Ltd., Wuhan, China). The test on the selective sensing of EP was performed in the presence of dopamine (DA), D-glucose (Glu), ascorbic acid (AA), uric acid (UA) and acetaminophen (AP) used as interfering analytes.

### 3. Results and Discussion

The gold–ruthenium composite material was manufactured using a two-stage approach based on the LCLD method [34]. According to this approach, in the first stage, we fabricated gold microstructures by laser deposition on the glass surface. At the second stage, the obtained microstructures were modified with ruthenium by its deposition on the gold surface. Both metals were deposited upon irradiation at 532 nm and at the scanning speed of 5  $\mu\text{M/s}$ . The compositions of the plating solutions are presented in Table 1. Based on the nature of the photochemical reduction of metal complexes [35–37] and spectral properties of the gold and ruthenium complexes used in this work [29,38–40], it can be assumed that the laser deposition process of Au and Ru at 532 nm is thermally induced and the contribution of any photochemical reactions can be omitted.

The morphology of the resulting composite was investigated by scanning electron microscopy (SEM). Figure 2a–c show SEM images of the Au–Ru surface on the different scales. It can be seen from scanning electronic micrographs that the fabricated electrode material has a highly developed non-planar surface.

The composite morphology can be considered as a complex hierarchical structure. It represents a set of large-scale pores ranging from a few to several tens of microns in diameter (Figure 2a,b), individual spherical droplets of 70–150 nm (Figure 2c) and their agglomerates with a size of several hundred nanometers (Figure 2b, inset), as well as small-scale surface irregularities (zigzag cracks) of several nanometers in size (Figure 2b and c, see the surface of droplets and their agglomerates). EDX analysis (Figure 2d) showed that Au–Ru composite mainly consists of gold (53 wt.%) and ruthenium (21 wt.%). The presence of other elements in the EDX spectra such as carbon, oxygen, magnesium, sodium, potassium and chlorine can be referred to the substrate material (glass). According to the obtained results, it is possible to conclude that the first stage of synthesis led to the formation of porous gold microstructures. Further, during the second stage, the gold structures were modified with ruthenium. Ru is deposited on the surface of Au in the form of islands consisting of individual nano-scale droplets and their clusters. The presence of Ru in the observed spherical particles was confirmed by EDX (Figure 2c, inset).

The overall result of the EDX analysis is consistent with the XRD data. Figure 2e illustrates the XRD patterns of Au and Au–Ru microstructures. According to XRD, two metal phases observed in Au–Ru composite are gold and ruthenium. It should be mentioned that similar small zigzag irregularities in Ru-based structures were observed in our recent studies [32,33]. The highly developed morphology of these structures was confirmed by electrical impedance spectroscopy (EIS) and their good electrocatalytic activity was demonstrated with respect to enzyme-free dopamine sensing.

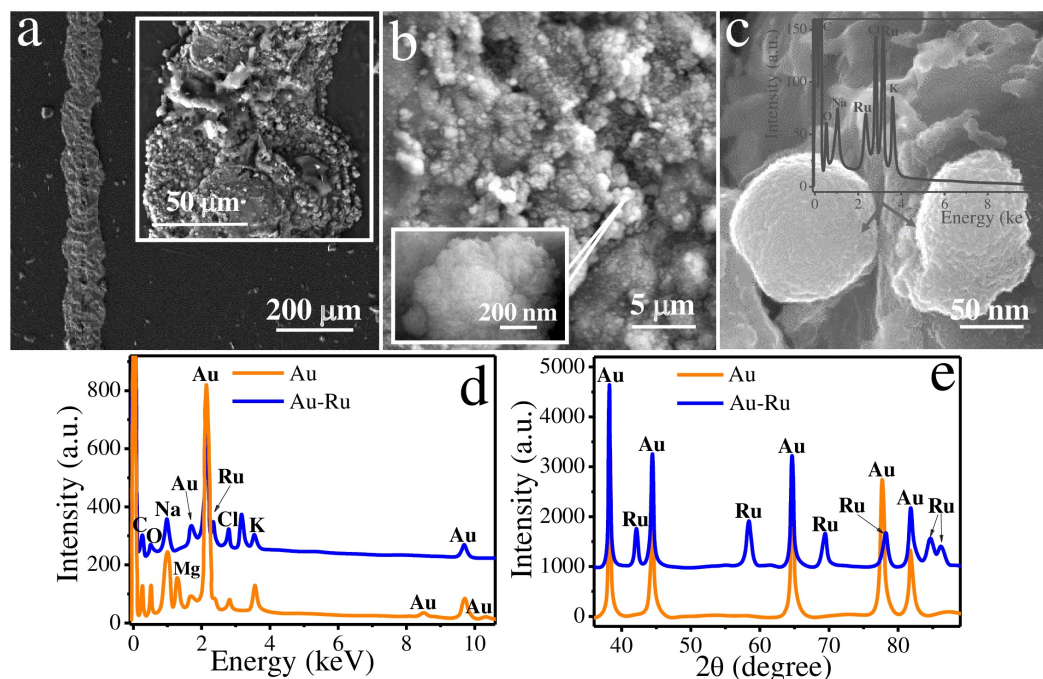


**Figure 2.** (a–c) SEM images of Au–Ru composite fabricated on glass. (d) EDX spectra and (e) XRD patterns of Au and Au–Ru microstructures. Morphological analysis demonstrated that the electrode material consists of porous gold microstructures with ruthenium particles irregularly distributed on their surface. These Ru particles have a highly developed structure with small zigzag cracks and exist in the form of either spherical droplets with a diameter of 70–150 nm (c) or their agglomerates with a size of several hundred nanometers (b, inset). EDX analysis showed that the main elements of the Au–Ru deposit are gold and ruthenium with weight percentages (wt.%) of 53 and 21, respectively.

In addition, the surface of the synthesized composite was also analyzed using the XPS method (Figure 3). Figure 3a presents two asymmetric peaks at  $\sim 84$  and  $\sim 87.7$  eV in the Au4f region with typical spin-orbit splitting of  $\sim 3.7$  eV [41] confirming the presence of Au<sup>0</sup>. On the other hand, Figure 3b reveals a doublet (asymmetric Ru3d<sub>5/2</sub> and Ru3d<sub>3/2</sub> peaks at  $\sim 279.8$  and  $\sim 284.0$  eV, respectively) in the Ru3d region with significant spin-orbit splitting of  $\sim 4.2$  eV, which can be assigned to the metallic ruthenium Ru<sup>0</sup> state [42]. Broadening of the Ru3d<sub>3/2</sub> peak can be due to strong overlap between the Ru3d and C1s regions [43].

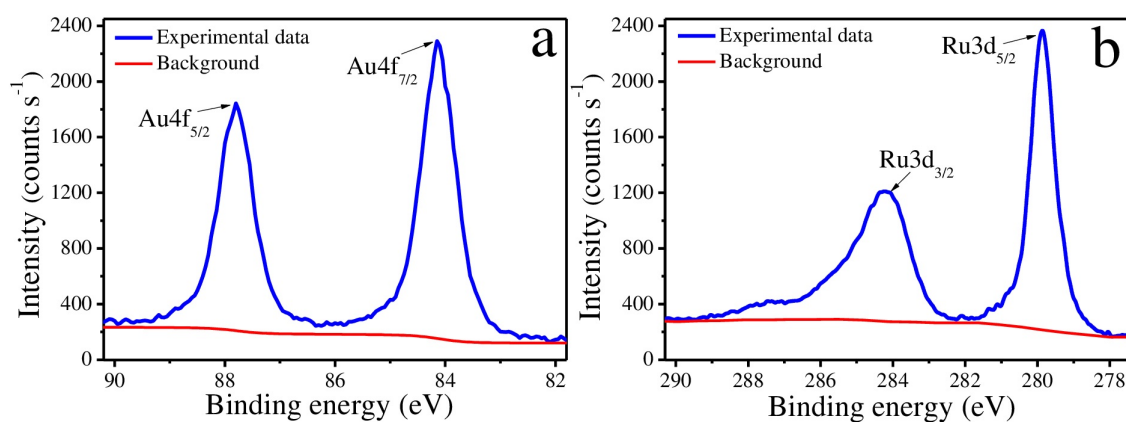


**Figure 3.** (a) Au4f and (b) Ru3d regions from XPS analysis of Au–Ru composite.

The electrochemical properties of Au–Ru composite were studied using methods of cyclic (CV) and differential pulse (DPV) voltammetry, as well as direct amperometry (Figure 4).

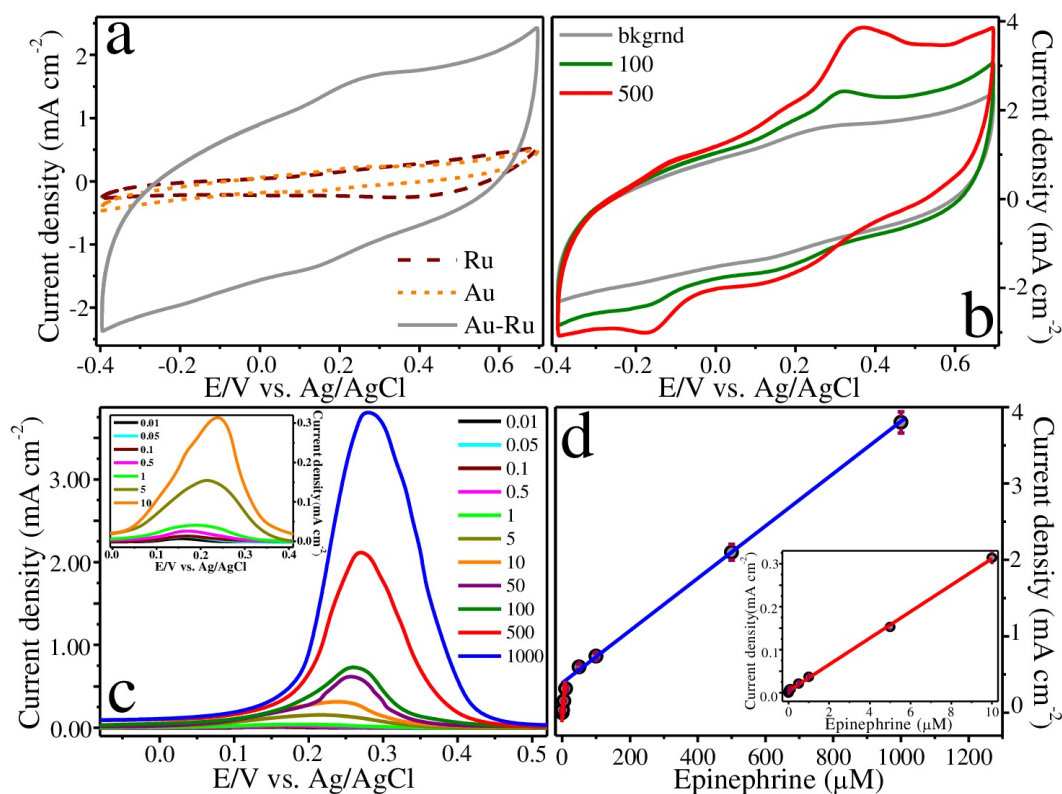


**Figure 4.** (a) CVs of Au, Ru, Au–Ru microstructures recorded in 0.1 M PBS. (b) CVs of Au–Ru microstructures recorded in 0.1 M PBS solution with epinephrine of two concentrations. (c) DPV curves of Au–Ru composite obtained in 0.1 M PBS containing different concentration of epinephrine. (d) Corresponding calibration curves of the electrocatalytic oxidation peak current as a function of the EP concentration. All concentrations in the legends are shown in  $\mu\text{M}$ .

The cyclic voltammograms (CVs) of bare gold and ruthenium electrodes together with gold-ruthenium electrode recorded in 0.1 M PBS are shown in Figure 4a. In general, the area of CV characterizes the charge flow via an electrode at certain concentration of analyte. Yet most importantly, the magnitude of the CV area is proportional to sensitivity of the electrode material toward the analyte of interest. Thus, from Figure 4a, it is clear that laser-assisted modification of Au with Ru dramatically increases the CV area in comparison with bare Au and Ru structures. These observations are in a good agreement with the results discussed in the previous paragraphs of this section.

Figure 4b illustrates CVs of Au–Ru composite in epinephrine solutions of various concentrations obtained in the potential range from  $-0.4$  to  $0.8$  V at scan rate of  $50$  mV/s. From Figure 4b, it is possible to distinguish at least two oxidation ( $0.16$  and  $0.35$  V) and two reduction ( $-0.16$  and  $0.17$  V) peaks. According to the literature [3,44,45], the possible mechanism for electrochemical oxidation of epinephrine can be presented as shown in Figure 5. As a result, the corresponding pairs of one-electron transfer processes can be attributed to the observed redox potentials as follows: (a) Broad peaks at  $0.16$  and  $0.35$  V correspond to oxidation of two hydroxyl groups of epinephrine with subsequent formation of epinephrinequinone. The potential difference can be caused by the different position of these group relative to other substituents in the benzene ring. (b) Broad peaks at  $-0.16$  and  $0.17$  V are related to reduction of epinephrinequinone to EP. (c) Another pair of one-electron transfer processes that involve reversible conversion between the chemically formed leucoadrenochrome and adrenochrome might be observed at higher (oxidation, at  $>0.6$  V) and lower (reduction, at  $<-0.3$  V) potentials.

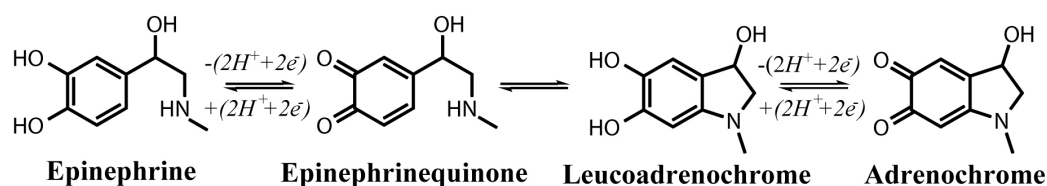


**Figure 5.** The possible mechanism for electrochemical oxidation of epinephrine [45].

It is known that differential pulse voltammetry (DPV) is a traditional method with relatively high current sensitivity and resolution, and it can be successfully used for the detection of analytes with lower concentrations. Figure 4c demonstrates DPV curves of gold-ruthenium electrode obtained in 0.1 M PBS for different epinephrine concentrations. As the concentration of EP increases from 0.01 to 1000  $\mu\text{M}$ , the intensity of the DPV signal progressively increases with a slight shift towards higher potentials. Afterwards, two linear calibration curves within 0.01–10  $\mu\text{M}$  ( $R = 0.9992$ ) and 10–1000  $\mu\text{M}$  ( $R = 0.9981$ ) were plotted using DPV data (Figure 4d). The presence of two linear regions might be explained by the hierarchical surface of Au–Ru electrode composed of two types of pores. In this regard, we assumed that high sensitivity observed at low EP concentrations (up to 10  $\mu\text{M}$ ) was provided by the smallest pores (zigzag irregularities on the surface Ru structures), whereas at higher concentrations of EP (more than 10  $\mu\text{M}$ ), the observed sensitivity was much lower. This could be a result of a stronger adsorption of the intermediates, e.g., adrenochrome (Figure 5), which are formed as a reaction of EP oxidation proceeds [45,46]. The estimated sensitivities within two linear ranges were 32.8 and 3.3  $\mu\text{A } \mu\text{M}^{-1} \text{ cm}^{-2}$ , respectively. The limits of detection ( $\text{LOD} = 3S/b$ , where  $S$  is the standard deviation from linearity, whereas  $b$  is the slope of the calibration curve, i.e., sensitivity) for two linear ranges were calculated to be 9 and 20 nM, respectively. The sensitivity of the majority of the reported amperometric sensors used for detection of hydrophobic metabolites typically lies between 1–10  $\mu\text{A } \mu\text{M}^{-1} \text{ cm}^{-2}$  [3,47]. In our case, we were able to fabricate the electrode material that has higher sensitivity within the range of low epinephrine concentrations. Further, the characteristics of Au–Ru electrode were compared with those of different similar sensors utilized for the epinephrine detection. The comparison results are summarized in Table 2.

**Table 2.** Comparison of the electrochemical performances of different epinephrine sensors.

Electrode Material	Linear Range ( $\mu\text{M}$ )	LOD ( $\mu\text{M}$ )	Refs.
Au–Ru composite	0.01–10 and 10–1000	0.009 and 0.02	This work
Au nanotube	10–150	2.8	[7]
Au–Pd core-shell nanocrystals	0.001–1000	0.0012	[16]
Pen/Au electrode	10–100 and 0.5–1	0.1	[44]
Nanoporous spongelike Au–Ag films	25–700	5.05	[45]
Poly(BCG)AuNp/GCE	4–903	0.01	[48]
PPY/ZnO/AuNp/RGO/GCE	0.6–500	0.06	[49]
Au-PILs-PPyNTs	35–960	0.2989	[50]

Thus, the electrode material fabricated in this work has better performance than many other epinephrine sensors that can be due to its well-developed morphology and catalytic synergy between Au and Ru.

Selectivity is an important characteristic for analyte detection in the physiological environment. We tested the selectivity of Au–Ru electrode towards non-enzymatic EP sensing in the presence of several physiological substances, including 50  $\mu\text{M}$  dopamine (DA), 50  $\mu\text{M}$  acetaminophen (AP), 50  $\mu\text{M}$  D-glucose (Glu), 50  $\mu\text{M}$  uric acid (UA) and 50  $\mu\text{M}$  ascorbic acid (AA) (Figure 6a). According to the obtained results, the current caused by addition of EP was much higher than response from adding the interfering species. Therefore, the studied Au–Ru electrode has rather good selectivity for the specific EP sensing.

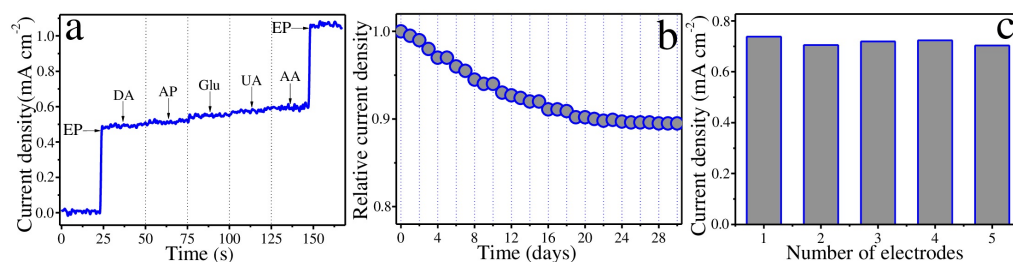


**Figure 6.** (a) Interference test of Au–Ru electrode in 0.1 M PBS (pH 7.0) at a working potential of 0.28 V with 100  $\mu\text{M}$  epinephrine (EP) and other interfering analytes, including 50  $\mu\text{M}$  dopamine (DA), 50  $\mu\text{M}$  acetaminophen (AP), 50  $\mu\text{M}$  D-glucose (Glu), 50  $\mu\text{M}$  uric acid (UA) and 50  $\mu\text{M}$  ascorbic acid (AA). (b) Long-term stability of Au–Ru electrode towards non-enzymatic epinephrine sensing investigated during one month. (c) The results of the reproducibility test obtained for five electrodes.

The long-term stability of Au–Ru electrode stored at room temperature and atmospheric pressure was evaluated by measuring the relative current density  $I_x/I_1$ , where  $I_x$  and  $I_1$  are the amperometric responses of Au–Ru with respect to 100  $\mu\text{M}$  epinephrine measured on the first day and each following day during one month, respectively (Figure 6b). As a result, it was shown that the relative current density remained above 88% of its initial value after one month of the evaluation. The latter means that the fabricated electrode exhibits an appropriate level of stability.

The good reproducibility of the electrochemical properties of Au–Ru composite were demonstrated by a low relative standard deviation (RSD less than 2.02%) in measuring the amperometric current of five electrodes in 100  $\mu\text{M}$  solution of EP (Figure 6c).

#### 4. Conclusions

In the current work, the synthesis of conductive porous Au–Ru composite was performed using a two-stage laser-assisted metal deposition technique. The main idea of the proposed approach was to deposit gold structures on glass with subsequent modification of their surface with ruthenium. Such modification resulted in fabrication of the composite material based on Au and Ru with much higher specific surface area than those of bare Au or Ru structures. The composite morphology has a complex hierarchical structure comprising of a set of large-scale pores ranging from a few to several tens of microns in diameter, individual spherical ruthenium droplets of 70–150 nm and their agglomerates with a size of several hundred nanometers. Ruthenium droplets and their clusters with small-scale surface irregularities (zigzag cracks) of several nanometers unevenly distributed along the surface of porous Au structures. A highly developed morphology of the fabricated Au–Ru composite determined its electrochemical behaviour that was examined using voltammetric methods. It was shown that Au–Ru sensor exhibits two linear ranges of the EP detection lying between 0.01 and 10  $\mu\text{M}$  and between 10 and 1000  $\mu\text{M}$ . The estimated sensitivities within two linear ranges were 32.8 and 3.3  $\mu\text{A } \mu\text{M}^{-1} \text{ cm}^{-2}$ , respectively. The limits of detection for two linear ranges were calculated to be 9 and 20 nM, respectively. Moreover, the fabricated electrode material demonstrated rather good selectivity, stability and reproducibility. Thus, Au–Ru composite revealed excellent electrocatalytic performance suitable for non-enzymatic sensing of such important hydrophobic metabolites as epinephrine.

**Author Contributions:** Conceptualization, M.S.P. and M.N.R.; methodology, A.P.Z. and M.S.P.; validation, M.S.P., A.V.V. and M.N.R.; investigation, A.P.Z., E.M.K., I.I.T. and M.S.P.; data curation A.P.Z., A.S.M., D.M.N. and M.S.P.; writing—original draft preparation, M.S.P.; writing—review and editing, M.S.P., A.V.V. and M.N.R.; project administration, M.S.P. and M.N.R.; funding acquisition, M.N.R. All authors have read and agreed to the published version of the manuscript.

**Funding:** This study was supported by Russian Science Foundation (project № 20-13-00303). Morphology and composition analysis investigation were partially funded by the Ministry of Science and Higher Education of the Russian Federation as part of World-class Research Center program: Advanced Digital Technologies (contract No. 075-15-2022-311 dated by 20.04.2022).



**Institutional Review Board Statement:** Not applicable

**Informed Consent Statement:** Not applicable

**Data Availability Statement:** Not applicable

**Acknowledgments:** The authors express their gratitude to the Research park of St. Petersburg State University “Interdisciplinary Resource Center for Nanotechnologies”, “Center for Magnetic Resonance”, “Center for Optical and Laser Research”, “Center for X-ray Diffraction Studies”, “Centre for Physical Methods of Surface Investigation”, “Center for Chemical Analysis and Materials Research”. The authors also acknowledge computational resources of Peter the Great Saint-Petersburg Polytechnic University Supercomputing Center ([www.spbstu.ru](http://www.spbstu.ru) (accessed on 30 November 2022)). The authors also acknowledge the Federal Joint Research Center “Material science and characterization in advanced technology” for providing SEM characterization.

**Conflicts of Interest:** The authors declare no conflict of interest.

## References

1. Heikenfeld, J.; Jajack, A.; Rogers, J.; Gutruf, P.; Tian, L.; Pan, T.; Li, R.; Khine, M.; Kim, J.; Wang, J. Wearable sensors: Modalities, challenges, and prospects. *Lab Chip* **2018**, *18*, 217–248.
2. Veerakumar, P.; Hung, S.T.; Hung, P.Q.; Lin, K.C. Review of the design of ruthenium-based nanomaterials and their sensing applications in electrochemistry. *J. Agric. Food Chem.* **2022**, *70*, 8523–8550.
3. Panahi, Z.; Custer, L.; Halpern, J.M. Recent advances in non-enzymatic electrochemical detection of hydrophobic metabolites in biofluids. *Sens. Actuators Rep.* **2021**, *3*, 100051.
4. Muthukumar, P.; Sumathi, C.; Wilson, J.; Ravi, G. Enzymeless biosensor based on  $\beta$ -NiS@ rGO/Au nanocomposites for simultaneous detection of ascorbic acid, epinephrine and uric acid. *RSC Adv.* **2016**, *6*, 96467–96478.
5. Anithaa, A.; Asokan, K.; Sekar, C. Voltammetric determination of epinephrine and xanthine based on sodium dodecyl sulphate assisted tungsten trioxide nanoparticles. *Electrochim. Acta* **2017**, *237*, 44–53.
6. Bonyadi, S.; Ghanbari, K.; Ghiasi, M. All-electrochemical synthesis of a three-dimensional mesoporous polymeric GC 3 N 4/PANI/CdO nanocomposite and its application as a novel sensor for the simultaneous determination of epinephrine, paracetamol, mefenamic acid, and ciprofloxacin. *New J. Chem.* **2020**, *44*, 3412–3424.
7. Wierzbicka, E.; Szultka-Młyńska, M.; Buszewski, B.; Sulka, G.D. Epinephrine sensing at nanostructured Au electrode and determination its oxidative metabolism. *Sens. Actuators Chem.* **2016**, *237*, 206–215.
8. Gorczyński, A.; Kubicki, M.; Szymkowiak, K.; Łuczak, T.; Patroniak, V. Utilization of a new gold/Schiff-base iron (III) complex composite as a highly sensitive voltammetric sensor for determination of epinephrine in the presence of ascorbic acid. *RSC Adv.* **2016**, *6*, 101888–101899.
9. Gao, Y.; Li, L.; Zhang, X.; Wang, X.; Ji, W.; Zhao, J.; Ozaki, Y. CTAB-triggered Ag aggregates for reproducible SERS analysis of urinary polycyclic aromatic hydrocarbon metabolites. *Chem. Commun.* **2019**, *55*, 2146–2149.
10. Li, W.; Wu, F.; Dai, Y.; Zhang, J.; Ni, B.; Wang, J. Poly (octadecyl methacrylate-co-trimethylolpropane trimethacrylate) monolithic column for hydrophobic in-tube solid-phase microextraction of chlorophenoxy acid herbicides. *Molecules* **2019**, *24*, 1678.
11. Bakker, E.; Telting-Diaz, M. Electrochemical sensors. *Anal. Chem.* **2002**, *74*, 2781–2800.
12. Revathi, C. Enzymatic and nonenzymatic electrochemical biosensors. In *Fundamentals and Sensing Applications of 2D Materials*; Elsevier: Amsterdam, The Netherlands, 2019; pp. 259–300.
13. Florescu, M.; David, M. Tyrosinase-based biosensors for selective dopamine detection. *Sensors* **2017**, *17*, 1314.
14. Ferri, S.; Kojima, K.; Sode, K. Review of glucose oxidases and glucose dehydrogenases: A bird’s eye view of glucose sensing enzymes. *J. Diabetes Sci. Technol.* **2011**, *5*, 1068–1076.
15. Yue, H.Y.; Zhang, H.J.; Huang, S.; Gao, X.; Song, S.S.; Wang, Z.; Wang, W.Q.; Guan, E.H. A novel non-enzymatic dopamine sensors based on NiO-reduced graphene oxide hybrid nanosheets. *J. Mater. Sci. Mater. Electron.* **2019**, *30*, 5000–5007.
16. Dong, W.; Ren, Y.; Bai, Z.; Jiao, J.; Chen, Y.; Han, B.; Chen, Q. Synthesis of tetrahedral Au-Pd core-shell nanocrystals and reduction of graphene oxide for the electrochemical detection of epinephrine. *J. Colloid Interface Sci.* **2018**, *512*, 812–818.
17. Wang, K.; Wu, C.; Wang, F.; Liao, M.; Jiang, G. Bimetallic nanoparticles decorated hollow nanoporous carbon framework as nanozyme biosensor for highly sensitive electrochemical sensing of uric acid. *Biosens. Bioelectron.* **2020**, *150*, 111869.
18. Tooley, C.A.; Gasperoni, C.H.; Marnoto, S.; Halpern, J.M. Evaluation of metal oxide surface catalysts for the electrochemical activation of amino acids. *Sensors* **2018**, *18*, 3144.
19. Hwang, D.W.; Lee, S.; Seo, M.; Chung, T.D. Recent advances in electrochemical non-enzymatic glucose sensors—A review. *Anal. Chim. Acta* **2018**, *1033*, 1–34.
20. Lopa, N.S.; Rahman, M.M.; Ahmed, F.; Ryu, T.; Sutradhar, S.C.; Lei, J.; Kim, J.; Kim, D.H.; Lee, Y.H.; Kim, W. Simple, low-cost, sensitive and label-free aptasensor for the detection of cardiac troponin I based on a gold nanoparticles modified titanium foil. *Biosens. Bioelectron.* **2019**, *126*, 381–388.
21. Li, G.; Xia, Y.; Tian, Y.; Wu, Y.; Liu, J.; He, Q.; Chen, D. Recent developments on graphene-based electrochemical sensors toward nitrite. *J. Electrochem. Soc.* **2019**, *166*, B881.

22. Arvand, M.; Khoshkholgh, Z.; Hemmati, S. Trace level detection of guanine and adenine and evaluation of damage to DNA using electro-synthesised ZnS@ CdS core-shell quantum dots decorated graphene oxide nanocomposite. *J. Electroanal. Chem.* **2018**, *817*, 149–159.
23. Li, G. Direct laser writing of graphene electrodes. *J. Appl. Phys.* **2020**, *127*, 010901.
24. Mizoshiri, M.; Nishitani, K.; Hata, S. Effect of heat accumulation on femtosecond laser reductive sintering of mixed CuO/NiO nanoparticles. *Micromachines* **2018**, *9*, 264.
25. Yang, Y.L.; Hsu, C.C.; Chang, T.L.; Kuo, L.S.; Chen, P.H. Study on wetting properties of periodical nanopatterns by a combinative technique of photolithography and laser interference lithography. *Appl. Surf. Sci.* **2010**, *256*, 3683–3687.
26. Zhang, J.; Chaker, M.; Ma, D. Pulsed laser ablation based synthesis of colloidal metal nanoparticles for catalytic applications. *J. Colloid Interface Sci.* **2017**, *489*, 138–149.
27. Gao, J.; Shao, C.; Shao, S.; Bai, C.; Khalil, U.R.; Zhao, Y.; Jiang, L.; Qu, L. Laser-assisted multiscale fabrication of configuration-editable supercapacitors with high energy density. *ACS Nano* **2019**, *13*, 7463–7470.
28. Lozhkina, O.A.; Panov, M.S.; Logunov, L.S.; Tumkin, I.I.; Gordeychuk, D.I.; Kochemirovsky, V.A. Aluminum chloride reveals the catalytic activity towards laser-induced deposition of copper from water-based solutions. *Int. J. Electrochem. Sci.* **2015**, *10*, 6084–6091.
29. Panov, M.S.; Khairullina, E.M.; Vshivtcev, F.S.; Ryazantsev, M.N.; Tumkin, I.I. Laser-induced synthesis of composite materials based on iridium, gold and platinum for non-enzymatic glucose sensing. *Materials* **2020**, *13*, 3359.
30. Barauskaite, V.E.; Novomlinskii, M.O.; Tumkin, I.I.; Khairullina, E.M.; Mereshchenko, A.S.; Balova, I.A.; Panov, M.S.; Kochemirovsky, V.A. In situ laser-induced synthesis of gas sensing microcomposites based on molybdenum and its oxides. *Compos. Part Eng.* **2019**, *157*, 322–330.
31. Panov, M.S.; Vereshchagina, O.A.; Ermakov, S.S.; Tumkin, I.I.; Khairullina, E.M.; Skripkin, M.Y.; Mereshchenko, A.S.; Ryazantsev, M.N.; Kochemirovsky, V.A. Non-enzymatic sensors based on in situ laser-induced synthesis of copper-gold and gold nano-sized microstructures. *Talanta* **2017**, *167*, 201–207.
32. Panov, M.S.; Grishankina, A.E.; Stupin, D.D.; Lihachev, A.I.; Mironov, V.N.; Strashkov, D.M.; Khairullina, E.M.; Tumkin, I.I.; Ryazantsev, M.N. In situ laser-induced fabrication of a ruthenium-based microelectrode for non-enzymatic dopamine sensing. *Materials* **2020**, *13*, 5385.
33. Stupin, D.D.; Abelit, A.A.; Mereshchenko, A.S.; Panov, M.S.; Ryazantsev, M.N. Copper–Ruthenium Composite as Perspective Material for Bioelectrodes: Laser-Assisted Synthesis, Biocompatibility Study, and an Impedance-Based Cellular Biosensor as Proof of Concept. *Biosensors* **2022**, *12*, 527.
34. Kochemirovsky, V.A.; Skripkin, M.Y.; Tveryanovich, Y.S.; Mereshchenko, A.S.; Gorbunov, A.O.; Panov, M.S.; Tumkin, I.I.; Safonov, S.V. Laser-induced copper deposition from aqueous and aqueous–organic solutions: State of the art and prospects of research. *Russ. Chem. Rev.* **2015**, *84*, 1059.
35. Khan, M.; Bouet, G.; Vierling, F.; Meullemeestre, J.; Schwing, M.J. Formation of cobalt (II), nickel (II) and copper (II) chloro complexes in alcohols and the Irving-Williams order of stabilities. *Transit. Met. Chem.* **1996**, *21*, 231–234.
36. Ryazantsev, M.N.; Jamal, A.; Maeda, S.; Morokuma, K. Global investigation of potential energy surfaces for the pyrolysis of C 1–C 3 hydrocarbons: Toward the development of detailed kinetic models from first principles. *Phys. Chem. Chem. Phys.* **2015**, *17*, 27789–27805.
37. Glebov, E.; Plyusnin, V.; Grivin, V.; Krupoder, S.; Liskovskaya, T.; Danilovich, V. Photochemistry of copper (II) polyfluorocarboxylates and copper (II) acetate as their hydrocarbon analogues. *J. Photochem. Photobiol. Chem.* **2000**, *133*, 177–183.
38. Parker, D.S.; Dangi, B.B.; Kaiser, R.I.; Jamal, A.; Ryazantsev, M.; Morokuma, K. Formation of 6-Methyl-1, 4-dihydronaphthalene in the Reaction of the p-Tolyl Radical with 1, 3-Butadiene under Single-Collision Conditions. *J. Phys. Chem.* **2014**, *118*, 12111–12119.
39. Bag, A.; Ghorai, P.K. Computational investigation of the ligand field effect to improve the photoacoustic properties of organometallic carbonyl clusters. *RSC Adv.* **2015**, *5*, 31575–31583.
40. El-Khoury, P.Z.; Tarnovsky, A.N.; Schapiro, I.; Ryazantsev, M.N.; Olivucci, M. Structure of the photochemical reaction path populated via promotion of CF2I2 into its first excited state. *J. Phys. Chem.* **2009**, *113*, 10767–10771.
41. Casaletto, M.; Longo, A.; Martorana, A.; Prestianni, A.; Venezia, A. XPS study of supported gold catalysts: The role of Au0 and Au+  $\delta$  species as active sites. *Surf. Interface Anal. Int. J. Devoted Dev. Appl. Tech. Anal. Surfaces, Interfaces Thin Film.* **2006**, *38*, 215–218.
42. Morgan, D.J. Resolving ruthenium: XPS studies of common ruthenium materials. *Surf. Interface Anal.* **2015**, *47*, 1072–1079.
43. Park, K.; Doub, J.; Gougousi, T.; Parsons, G. Microcontact patterning of ruthenium gate electrodes by selective area atomic layer deposition. *Appl. Phys. Lett.* **2005**, *86*, 051903.
44. Wang, L.; Bai, J.; Huang, P.; Wang, H.; Zhang, L.; Zhao, Y. Electrochemical behavior and determination of epinephrine at a penicillamine self-assembled gold electrode. *Int. J. Electrochem. Sci.* **2006**, *1*, 238–249.
45. Wierzbicka, E.; Sulka, G.D. Nanoporous spongelike Au–Ag films for electrochemical epinephrine sensing. *J. Electroanal. Chem.* **2016**, *762*, 43–50.
46. Zhu, D.; Ma, H.; Zhen, Q.; Xin, J.; Tan, L.; Zhang, C.; Wang, X.; Xiao, B. Hierarchical flower-like zinc oxide nanosheets in-situ growth on three-dimensional ferrocene-functionalized graphene framework for sensitive determination of epinephrine and its oxidation derivative. *Appl. Surf. Sci.* **2020**, *526*, 146721.
47. Lakard, S.; Pavel, I.A.; Lakard, B. Electrochemical biosensing of dopamine neurotransmitter: A review. *Biosensors* **2021**, *11*, 179.

48. Taei, M.; Hadadzadeh, H.; Hasanpour, F.; Tavakkoli, N.; Dolatabadi, M.H. Simultaneous electrochemical determination of ascorbic acid, epinephrine, and uric acid using a polymer film-modified electrode based on Au nanoparticles/poly (3,3',5,5'-tetrabromo-m-cresolsulfonphthalein). *Ionics* **2015**, *21*, 3267–3278.
49. Ghanbari, K.; Hajian, A. Electrochemical characterization of Au/ZnO/PPy/RGO nanocomposite and its application for simultaneous determination of ascorbic acid, epinephrine, and uric acid. *J. Electroanal. Chem.* **2017**, *801*, 466–479.
50. Mao, H.; Zhang, H.; Jiang, W.; Liang, J.; Sun, Y.; Zhang, Y.; Wu, Q.; Zhang, G.; Song, X.M. Poly (ionic liquid) functionalized polypyrrole nanotubes supported gold nanoparticles: An efficient electrochemical sensor to detect epinephrine. *Mater. Sci. Eng.* **2017**, *75*, 495–502.